AN EVALUATION OF IMAGE DENOISING TECHNIQUES APPLIED TO CT BAGGAGE SCREENING IMAGERY

Andre Mouton, Greg T. Flitton, Suzanne Bizot, Najla Megherbi, Toby P. Breckon
School of Engineering, Cranfield University, Bedfordshire, UK.

ABSTRACT

This paper investigates the efficacy of several popular denoising methods in the previously unconsidered context of Computed Tomography (CT) baggage imagery. The performance of a dedicated CT baggage denoising approach (alpha-weighted mean separation and histogram equalisation) is compared to the following popular denoising techniques: anisotropic diffusion; total variation denoising; bilateral filtering; translation invariant wavelet shrinkage and non-local means filtering. In addition to a standard qualitative performance analysis (visual comparisons), denoising performance is evaluated with a recently developed 3D SIFT-based analysis technique that quantifies the impact of denoising on the implementation of automated 3D object recognition. The study yields encouraging results in both the qualitative and quantitative analyses, with wavelet thresholding producing the most satisfactory results. The results serve as a strong indication that simple denoising will aid human and computerised analyses of 3D CT baggage imagery for transport security screening.

Index Terms— Image denoising, baggage CT, 3D SIFT

1. INTRODUCTION

Traditionally, X-ray based 2D imaging technologies have been used for the real-time scanning of bags in the airport security and/or parcel handling settings. Recent technological advances however, have allowed for the employment of dual-energy CT scanners and hence the availability of 3D imagery for these purposes [1, 2] (see Figure 1). For both technologies (X-ray and CT), screening for weapons and complex contraband objects is performed by human operators, while automated detection is generally limited to materials-based explosives discrimination [2]. Recent studies have investigated the implementation of computer vision techniques, such as automatic object recognition, in the domain of 3D baggage screening [3–5]. Such techniques however, have been shown to be severely hindered by the high degrees of noise and artefacts common in CT baggage imagery [3, 6].

Despite the abundance of image-processing literature in the area of medical CT, similar research related to industrial applications and baggage screening in particular, are very limited [3, 6, 7]. Medical CT images are generally of a much higher quality than those obtained in the security screening sector. This is primarily due to the fact that the CT scanners used to capture CT volumetric baggage imagery, are aimed at dual energy explosives detection and not at object recognition, as is the case in the medical setting [2]. Subsequently, the CT baggage images present with substantial noise, streaking artefacts (resulting from the presence of metal items) and poor resolution [6].

Zhou *et al.* [7, 8] examine the noise properties of CT baggage scans in particular. They observe that due to the very high dynamic range of the images, the non-object (i.e. background) regions often appear dark, despite exhibiting non-zero pixel values. As a result, much of the background noise in the images is not visible under normal circumstances. Image enhancement, using Histogram Equalisation (HE) [9] however, reduces the effective dynamic range of the image and often reveals high degrees of background projection noise (see Figure 2). The authors proceed to use image enhancement to remove this noise and improve the resolution in CT baggage imagery. Performance analysis however, seems to be focussed predominantly on the improvement in image contrast and little mention is made regarding the effectiveness of the denoising stage of the technique (particularly from a quantitative perspective). It is also worth noting that the images used in the study [8] are largely free of streaking artefacts, and the efficacy of the method in the presence of metal artefacts is thus unclear.

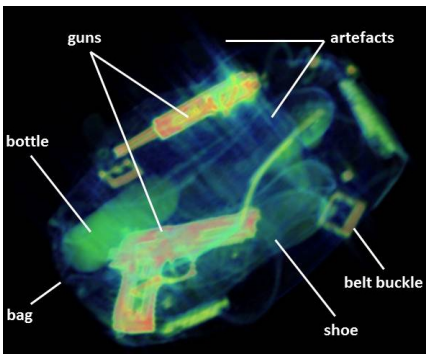

Fig. 1. Example volumetric CT scan of a piece of baggage containing two firearms in a cluttered environment.

Besides this work of Zhou *et al.* [7, 8], previous studies regarding the denoising of complex baggage imagery of this nature, containing dense collections of man made objects scanned at low resolution and in the presence of noise and metal artefacts, are extremely limited. There is evidence in the medical literature however, that simple denoising operations can significantly improve the quality of CT images and benefit subsequent, more complex operations [10–13]. The value of such techniques when applied to CT baggage imagery has not been considered previously and is worth investigating.

This work thus extends the previous work of Zhou *et al.* [7, 8] by comparing the performance of several popular denoising techniques within the previously unconsidered context of CT baggage imagery. In particular, the potential benefits of denoising on the application of more complex operations within this context, including volume rendering and automatic object recognition algorithms, are evaluated.

2. 3D CT BAGGAGE IMAGERY

As the vast majority of CT-based literature considers medical applications, it is important to emphasise that several key differences between typical medical CT data and baggage CT data mean that image processing techniques which have been successfully applied to medical images will not necessarily be successful when applied to non-medical CT images.

This project was funded under the Innovative Research Call in Explosives and Weapons Detection (2010) initiative, a cross-government programme sponsored by a number of departments and agencies under the UK Government's CONTEST strategy, in partnership with US Department of Homeland Security. The authors are grateful for additional support from Reveal Imaging Technologies Inc. (USA).

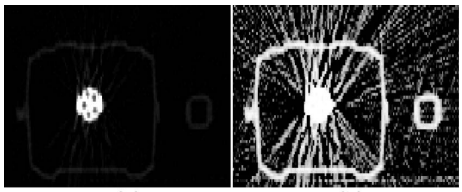

Fig. 2. CT baggage image slice before (a) and after (b) histogram equalisation. Histogram equalisation reveals the high degree of background projection noise, previously not visible.

While sub-millimetre isotropic resolutions in all three dimensions has become the norm in medical CT scanners [15, 16], the volumetric CT baggage data used in this study was obtained using a CT-80 baggage scanner manufactured by Reveal Imaging Inc. and yields an optimal spatial resolution of 1.56x1.61x5.00mm. Furthermore, the demand for a higher scan speed in the security screening setting (compared to the medical setting), leads to compromises in image quality in both resolution and noise [2]. The resolution of baggage data is thus anisotropic and significantly worse than the state of the art medical data. Anisotropic voxel resolution and poor resolution in the axial plane in particular, compound the effects of image noise and artefacts [17].

While medical CT scans generally present with relatively low degrees of complexity and contain minimal clutter, the content of a typical CT baggage scan is highly unpredictable and often extremely complex, exhibiting high degrees of clutter and artefact corruption [18] (see Figure 1). It is widely accepted that both human and computer detection rates are severely affected by complexity and clutter [2].

Previous studies, investigating the efficacy of denoising techniques when applied to low resolution imagery of this nature, containing dense collections of man made objects scanned in the presence of noise and metal artefacts, is extremely limited.

3. TECHNIQUES COMPARED

In addition to the approach of Zhou *et al.* [8], we use the recent denoising survey of Buades *et al.* [19] as a reference for selecting the denoising algorithms to compare. The following methods are thus selected for investigation: anisotropic diffusion; total variation denoising; bilateral filtering; translation invariant wavelet shrinkage; non-local means filtering and alpha-weighted mean separation and histogram equalisation.

Anisotropic diffusion: Anisotropic diffusion is a shape-adaptive filtering technique whereby an image is evolved under an edge controlled diffusion operator where the orientation of the filter is determined by the local gradient in the image. Image details such as edges and lines are thus preserved or even enhanced, while regions within edges are smoothed [20]. The generalised diffusion equation is given by:

$$\frac{\delta}{\delta t} I(x,y,t) = div(c(x,y,t)\nabla I(x,y,t)) \tag{1}$$

$$I(x,y,0) = I_0(x,y) \tag{2}$$

where ∇ denotes the image gradient, $div(...)$ is the divergence operator and $c(x,y,t)$ is the diffusivity function, controlling the rate of diffusion [20]. Perona and Malik [20] proposed that $c(x,y,t)$ be chosen as a function of the image gradient, such that image edges are preserved:

$$c(x,y,t) = 1/(1 + \frac{|\nabla I|^2}{K^2}) \tag{3}$$

where K is a contrast parameter and is determined automatically using the noise estimator described by Canny [21].

Total Variation (TV) denoising: TV denoising exploits the prinicple that reducing the total variation [22] of an image, while maintaining a close match to the original image, removes image noise, whilst simultaneously preserving important details such as edges [23–25]. Rudin *et al.* [22] define the total variation of an image, u, as:

$$J(u) = \sum_{1 \leq x,y \leq N} |(\nabla u)_{x,y}| \tag{4}$$

where $|u| := \sqrt{u_1^2 + u_2^2}$ for every $u = (u_1, u_2) \in \Re^2$. The total variation denoising problem can then be described as:

$$\min_{u \in X} \frac{\|u - g\|^2}{2\lambda} + J(u) \tag{5}$$

where $\|.\|$ is the 2D Euclidean norm and $\lambda > 0$ is a regularisation parameter. This study utilizes the iterative TV minimisation approach developed by Chambolle [25] to solve the above minimisation problem.

Bilateral filtering: The bilateral filter is another edge-preserving smoothing filter. The filter is defined by a Gaussian weighted average of pixels in a predefined local neighbourhood [26–28]. The technique is based on the principle that two pixels are similar not only if they are close to one another spatially but also if they exhibit some similarity in their photometric range or intensity [29]. The output pixel is thus computed as a weighted combination of its neighbouring pixels according to:

$$g(x,y) = \frac{\sum_{k,l} u(k,l) w(x,y,k,l)}{\sum_{k,l} w(x,y,k,l)} \tag{6}$$

where the weighting coefficient $w(x,y,k,l)$ is computed as the product of a *domain kernel* $d(x,y,k,l)$ and *range kernel* $r(x,y,k,l)$:

$$d(x,y,k,l) = exp(-\frac{(x-k)^2 + (y-l)^2}{2\sigma_d^2}) \tag{7}$$

$$r(x,y,k,l) = exp(-\frac{\|u(x,y) - u(k,l)\|^2}{2\sigma_r^2}) \tag{8}$$

Translation-invariant wavelet shrinkage: Coifman *et al.* [30] show that due to the lack of translation invariance of the wavelet basis, traditional wavelet denoising via thresholding, leads to visual artefacts in the denoised image. They present a modified approach to reduce these artefacts using a technique termed *cycle spinning* which averages out the translation dependence of the wavelet basis.

Non-Local Means (NLM) filtering: The NLM filter of Buades *et al.* [19, 31] computes the mean of the values of all points whose Gaussian neighbourhood looks like the neighbourhood of the current pixel. In a recent survey on image denoising techniques [19], the NLM filter outperformed several state of the art denoising techniques. In the NLM algorithm, the estimated value for a pixel at coordinates (x,y) is computed as a weighted average of all the pixels in the image:

$$g(x,y) = \frac{\sum_{k,l} w(x,y,k,l) u(k,l)}{\sum_{k,l} w(x,y,k,l)} \tag{9}$$

where the weights, $w(x,y,k,l)$, are computed based on the similarity of pixels $u(x,y)$ and $u(k,l)$:

$$w(x,y,k,l) = exp(-\frac{\|u(x,y) - u(k,l)\|_a^2}{h^2}) \tag{10}$$

where $\|u(x,y) - u(k,l)\|_a^2$ is a Gaussian weighted Euclidean norm and a is the standard deviation of the Gaussian kernel. The parameter h is a constant proportional to the estimated noise in the input image.

Alpha-Weighted Mean Separation and Histogram Equalisation (AWMSHE): Zhou *et al.* [8] present an image enhancement algorithm that combines alpha-weighted mean separation and histogram equalisation to remove background noise and improve the resolution in CT baggage imagery. The proposed algorithm is comprised of two stages: noise removal and image enhancement. The noise removal step exploits the fact that much of the projection noise present in CT baggage imagery is characterised by very low pixel values relative to the high dynamic range of the image. A simple threshold-type noise removal procedure thus seems promising. An initial 2D CT image I is separated into an object image I_O (containing the valuable information in the image) and a noise image I_N (comprised of only noise) via Alpha-Weighted Mean (AWM) thresholding:

$$I_O(x,y) = I(x,y) \quad \text{for} \quad I(x,y) \geq th_1 \tag{11}$$

$$I_N(x,y) = I(x,y) \quad \text{for} \quad I(x,y) < th_1 \tag{12}$$

where the noise threshold $th_1 = \alpha_1 I_{mean}$ and I_{mean} is the mean pixel value of I. The noise image I_N is then discarded and the object image I_O is subdivided again into upper and lower image sub-images (I_U and I_L) by applying a second threshold $th_2 = \alpha_2 I_{O\_mean}$:

$$I_U(x,y) = I_O(x,y) \quad \text{for} \quad I_0(x,y) \geq th_2 \tag{13}$$

$$I_L(x,y) = I_O(x,y) \quad \text{for} \quad I_O(x,y) < th_2 \tag{14}$$

The upper image I_U contains the brighter regions of the object image, while the lower image I_L contains the darker (yet still informative) regions. I_L is enhanced via Histogram Equalisation (HE) [9] yielding an enhanced image E_L and I_U is clipped to the maximum value of I_L (to compress the data range without introducing new artefacts) yielding the upper enhanced image E_U. The final image E is then created by combining E_U and E_L via addition:

$$E(x,y) = E_U(x,y) + E_L(x,y) \tag{15}$$

4. METHODOLOGY

Evaluating the performance of a denoising algorithm is an essential yet challenging task. In reality, baggage screening is a human-operated task whereby a security official visually inspects every scan [18]. In other words, it is a qualitative problem. Therefore, emphasis should be placed on the qualitative analysis of the denoising algorithms.

The visual quality of the volumes before and after denoising are compared; this is done for both the original volumes as well as the original volumes corrupted with Gaussian noise of known standard deviation. An iso-surface based volume rendering technique [32], is applied to the data before and after filtering and the visual quality of the resulting volumes is used as an indication of the efficacy of the denoising technique.

Despite the importance of the qualitative analysis of the denoising algorithms, some form of quantitative analysis is still valuable. Traditionally, the mean-squared error (MSE) has been used to quantify the performance of reconstruction algorithms [9]. A recent study, however, has highlighted the limitations of using the MSE in the context of image processing [33]. The authors go as far as to say that the MSE is unreliable when used to predict human perception of image fidelity and quality. An alternative approach is thus desired.

A predominant motivation for effectively denoising CT baggage images is to aid the implementation of subsequent automated 3D object recognition. Flitton *et al.* [3] have investigated the implementation of object recognition in complex CT volumes based on 3D SIFT features. The study shows that the presence of CT artefacts and noise is the predominant factor contributing to false positives.

The recent quantitative performance analysis technique of Mouton *et al.* [34], which is based on 3D SIFT keypoints [3], is thus used to quantify the results of the denoising algorithms. The technique uses the recent 3D extension [3] to the traditional SIFT algorithm [35] to determine the locations of keypoints in the volumes before and after denoising. Keypoint locations are determined in a similar manner to their 2D counterparts. An initial candidate set of keypoints is taken as the local extrema of multi-scale Difference of Gaussian (DoG) volumes, where the DoG volumes are created by convolving the input volume $I(x,y,z)$ with 3D Gaussian filters $G(x,y,z,k\sigma)$ at different scales:

$$\begin{aligned} DoG(x,y,z,k) = I(x,y,z) \star G(x,y,z,k\sigma_s) \\ - I(x,y,z) \star G(x,y,z,(k-1)\sigma_s) \end{aligned} \tag{16}$$

where k is an integer representing the scale index. A voxel is then considered a local extrema if it is a minimum or maximum in its local 3 x 3 x 3 (i.e. 26 voxels) neighbourhood at the current scale k as well as in the 27 voxel neighbourhoods in the two adjacent scale space DoG volumes (i.e. at scales $(k+1)$ and $(k-1)$). This initial candidate set of keypoints is then refined by discarding unstable keypoints caused by poor contrast if their densities are below a given threshold τ_c. The candidate set is refined further by discarding the keypoints related to poor localisation on edges - determined by a second threshold τ_e related to the Trace and Determinant of the 3 x 3 Hessian matrix of the DoG volume [3].

This 3D SIFT point detector is run on the volume before and after denoising and the number of object and noise SIFT points are manually recorded. An object feature point is identified as one located on an object of interest within the CT image whilst a noise feature point is considered as one which is not on the primary object within the CT image (i.e. assumed to be caused by noise or artefacts). The ratio of object feature points to total feature points (object + noise) is used as an indication of the performance of the given technique. It is assumed that an increase in this ratio will ultimately correspond to improved object recognition results [34].

5. RESULTS

The aforementioned methods were tested on several scans obtained from a CT-80 model baggage scanner manufactured by Reveal Imaging Technologies. Since CT volumes are essentially composed of a set of CT slices, where each individual slice is a 2D image, the denoising algorithms could be implemented in the 2D domain by applying them on a 'per-slice' basis. The volumes were then reconstructed from the denoised slices. The optimal parameters for each of the denoising algorithms were determined empirically.

Figure 3 shows the results of applying the denoising algorithms to a scan of a container containing a single firearm. The first image in the figure displays the original, unfiltered volume and subsequent images (b) - (g) display the results of each of the denoising techniques. In Figure 3(a) the streaking artefacts surrounding the firearm in the centre of the container are clear. Each of the denoising methods yielded a significantly cleaner image. While the streaking artefacts are considerably reduced they are not completely removed. A greater degree of filtering would be required to remove more of the streaks but this would likely result in an undesired loss in valuable image information. It is thus apparent that denoising alone is not sufficient for removing all of the streaking artefacts without destroying image detail. This is especially evident for the AWMSHE approach

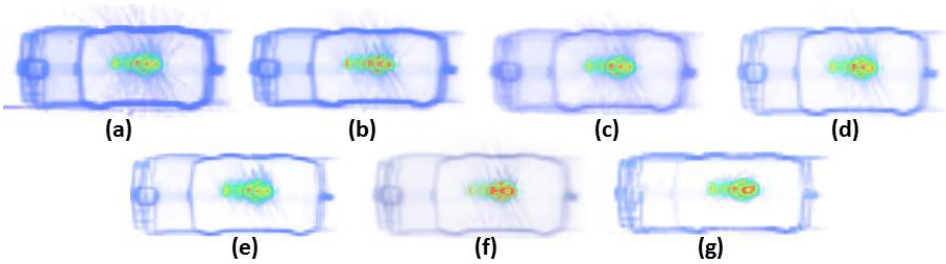

Fig. 3. (a) Original (b) Anisotropic diffusion (c) Bilateral filter (d) TV filter (e) Wavelet thresholding (f) NLM filter (g) AWMSHE

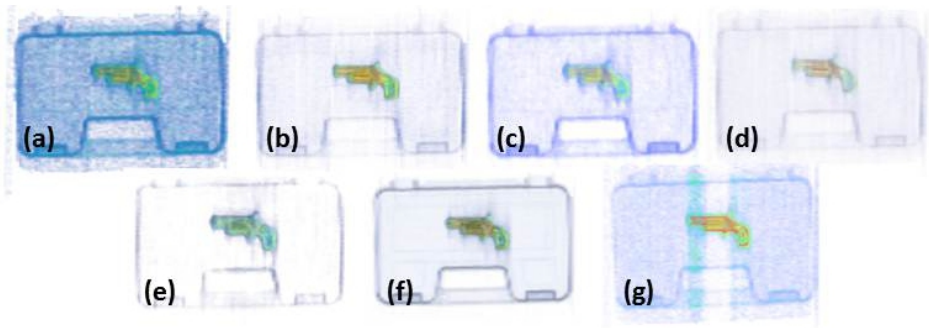

Fig. 4. (a) Original image with Gaussian noise, σ = 15 (b) Anisotropic diffusion (c) Bilateral filter (d) TV filter (e) Wavelet thresholding (f) NLM filter (g) AWMSHE

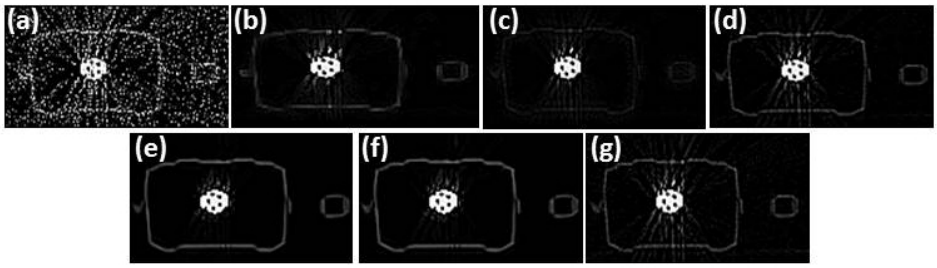

Fig. 5. Single slice analysis with Gaussian noise corruption. (a) Original image with Gaussian noise, σ = 15 (b) Anisotropic diffusion (c) Bilateral filter (d) TV filter (e) Wavelet thresholding (f) NLM filter (g) AWMSHE

(Figure 3 (g)) where the loss of edge information is clear. Recall that the AWMSHE approach relies on the noise being characterised by much lower pixel values than the 'valuable' image regions (containing important details) for denoising to be successful. Therefore, such a threshold-based denoising approach is bound to be insufficient for dealing with streak-like artefacts and heavy noise corruption as the required threshold will lead to significant destruction of edge information.

Figure 4 displays the same scan (in a different orientation), corrupted with Gaussian noise of standard deviation of 15 and then processed with each of the denoising methods. Figure 5 illustrates a single slice from each of the volumes in Figure 4. The variation in performance of the different algorithms is clearer in these two sets of figures. While this degree of noise corruption is unlikely in reality, it illustrates the efficacy of the denoising algorithms well. The NLM filter and wavelet shrinkage approach produced the most pleasing visual results, with the majority of the noise removed and a clear image of the firearm and container remaining. The limitations of simple denoising in terms of artefact removal are also illustrated clearer here: while the background noise is significantly reduced, considerable streaking artefacts remain - even for the two most effective methods (NLM filtering and wavelet thresholding). Interestingly, despite the fact that the AWMSHE approach is the only dedicated baggage CT denoising technique the results are perhaps the poorest - with considerable degrees of noise and artefacts remaining (Figure 4 (g) and Figure 5 (g)).

Figure 6 displays the results of the iso-surface based volume rendering algorithm [32], on the original scan and after applying each of the denoising algorithms. Wavelet thresholding and the NLM filter again yielded the most satisfactory results. To illustrate the effects of denoising on the rendering results more clearly, Figure 7 shows a magnified region of the rendered volumes before and after applying the NLM filter, which produced the most pleasing results. Denoising resulted in a considerably cleaner result, as is indicated by the demarcated regions.

Finally, Table 1 and Figure 8 display the results of the quantitative analysis discussed earlier. As mentioned, the SIFT point detection algorithm includes a refinement procedure whereby candidate SIFT points are rejected due to poor contrast and/or poor localisation on edges [3]. These rejections are governed by two thresholds which were set according to the optimal values recommended by Flitton *et al* [3]. The number of object and noise SIFT points was manually recorded across three scale-space levels. The results in Table 1 left indicate that there was no significant variation in the number of ob-

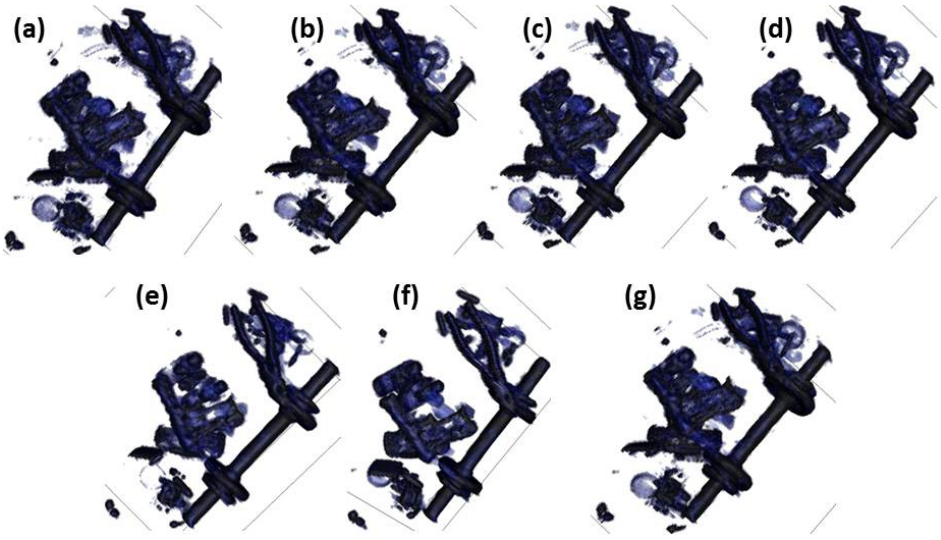

Fig. 6. Volume rendering on: (a) Original (b) Anisotropic diffusion (c) Bilateral filter (d) TV filter (e) Wavelet thresholding (f) NLM filter (g) AWMSHE

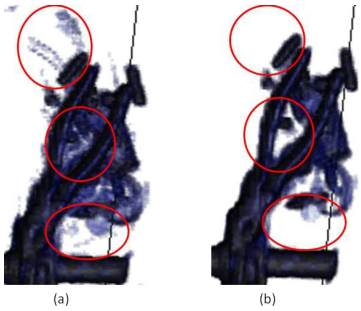

Fig. 7. Magnified region of rendered volumes for with regions of interest marked: (a) Original volume (b) NLM filtered volume

Method	Object points	Noise points	Ratio
Unfiltered	37	19	0.66
Anisotropic	27	8	0.77
Bilateral	33	2	0.94
TV	36	20	0.64
Wavelets	**35**	**0**	**1.00**
NLM	33	1	0.97
AWMSHE	26	8	0.76

Table 1. Results of quantitative analysis of denoising techniques showing: number of object and noise feature points and resulting ratios. The best performing method indicated in bold.

ject feature points detected for each of the volumes. For the unfiltered volume a total of 19 noise feature points was detected, yielding a ratio of 0.66. In every case, excluding TV filtering, denoising resulted in significantly fewer noise feature points and subsequently much higher ratios. Wavelet thresholding (indicated in bold in Table 1) yielded the optimal results with 0 noise feature points and thus a perfect ratio. The bilateral filter (2 noise feature points and ratio = 0.94) and NLM filter (1 noise feature point and ratio = 0.97) also returned statistically significant improvements. As was the case with the quantitative analysis, the AWMSHE was outperformed by the majority of the standard denoising techniques, indicating that this approach is of limited benefit in environments characterised by high degrees of artefacts and noise (the technique was tested on images with a much lower degree of artefacts and noise in the original work [8]).

For illustrative purposes, the SIFT point locations at the first scale-space level on the volumes before and after applying each of the denoising techniques are shown in Figure 8. The reduction in the number of noise feature points post-denoising is clear. These images illustrate keypoint locations at the first scale-space level only and so the numbers of object and noise feature points do not correspond directly with those in Table 1, which represent the numbers of keypoints across all three scale-space levels. The significant improvement in the ratio of object to total feature points, with little to no decline in the number of object feature points, is a strong indication that simple denoising will lead to improved object recognition results using techniques such as those implemented in [3].

6. CONCLUSIONS

This paper has compared the performance of several popular image denoising techniques in the previously unconsidered context of CT baggage imagery. In particular, images characterised by high degrees of background noise and streaking artefacts are considered. Previous studies considering the denoising of CT baggage scans are limited to the work of Zhou *et al.* [7, 8], where images with relatively low degrees of noise and artefacts are considered and no comparative analyses is performed. The major contribution of this study has thus been the extension of these previous works by considering low quality CT baggage imagery; by comparing the performance of a variety of simple, yet popular denoising algorithms, which have been met with success in other areas of image processing and by considering the impact of denoising on subsequent feature-based automated object recognition in this environment.

A comprehensive qualitative analysis indicated that all of the standard 2D denoising techniques yielded improvements in the visual quality of the volumes and significantly outperformed the dedicated CT baggage denoising approach of Zhou *et al.* [8].

A quantitative performance analysis using the technique of Mouton *et al.* [34] was used to quantify the impact of denoising

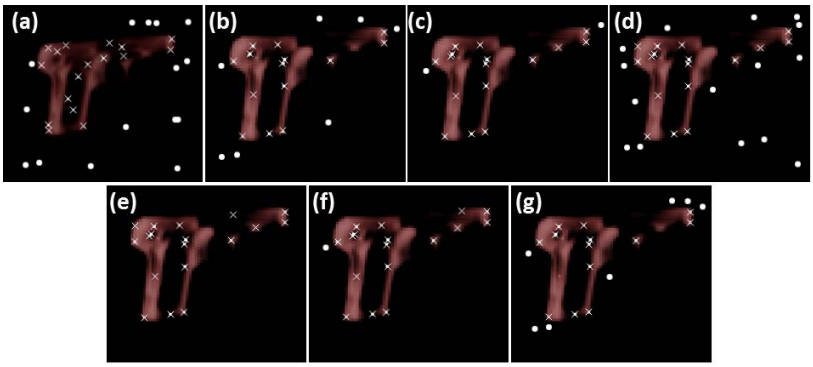

Fig. 8. SIFT point locations at the first scale space level (cross = object; dot = noise): (a) Original (b) Anisotropic diffusion (c) Bilateral filter (d) TV filter (e) Wavelet thresholding (f) NLM filter (g) AWMSHE

on subsequent feature-based automated object recognition. Performance evaluation using this technique showed considerable improvements, particularly for wavelet thresholding. The improvements observed in the quantitative analysis and improved volume rendering results for the NLM filter and wavelet thresholding, is a strong indication that these standard 2D denoising techniques will be benefit the implementation of complex computer vision techniques to CT baggage scans [3–5].

Future work will focus on a more detailed analysis of the impact of denoising on the performance of subsequent computer vision techniques such automated object recognition and segmentation in the CT baggage imagery domain.

7. REFERENCES

[1] B. R. Abidi, Y. Zheng, A. V. Gribok, and M. A. Abidi, "Improving weapon detection in single energy x-ray images through pseudocoloring," *IEEE Trans. on Systems, Man, and Cybernetics*, vol. 36, no. 6, pp. 784–796, 2006.

[2] S. Singh, "Explosives detection systems (EDS) for aviation security," *Signal Processing*, vol. 83, no. 1, pp. 31–55, Jan. 2003.

[3] G. Flitton, T.P. Breckon, and N. Megherbi, "Object recognition using 3D SIFT in complex CT volumes," in *Proc. British Machine Vision Conference*, 2010, pp. 11.1–11.12.

[4] N. Megherbi, G. T. Flitton, and T. P. Breckon, "A classifier based approach for the detection of potential threats in CT based baggage screening," in *ICIP*, 2010, pp. 1833–1836.

[5] G.T. Flitton, T.P. Breckon, and N. Megherbi, "A 3D Extension to Cortex Like Mechanisms for 3D Object Class Recognition," in *IEEE Proc. Inter. Conf. on Computer Vision and Pattern Recognition*, June 2012, pp. 3634–3641.

[6] J. F. Barrett and N. Keat, "Artifacts in CT: Recognition and avoidance," *Radiographics*, vol. 24, no. 6, pp. 1679, 2004.

[7] Y. Zhou, K. Panetta, and S. Agaian, "3D CT baggage image enhancement based on order statistic decomposition," in *Technologies for Homeland Security (HST), 2010 IEEE Inter. Conf. on*, 2010, pp. 287–291.

[8] Y. Zhou, K. Panetta, and S. Agaian, "CT baggage image enhancement using a combination of alpha-weighted mean separation and histogram equalization," in *Proc. SPIE*, 2010, vol. 7708, p. 77080G.

[9] C.J. Solomon and T.P. Breckon, *Fundamentals of Digital Image Processing: A Practical Approach with Examples in Matlab*, Wiley-Blackwell, 2010.

[10] J. Hsieh, *Computed tomography: principles, design, artifacts, and recent advances*, SPIE and John Wiley and Sons, 2003.

[11] E. Seeram, *Computed tomography: physical principles, clinical applications, and quality control*, WB Saunders, 2001.

[12] H. Yu, K. Zeng, D. K. Bharkhada, G. Wang, M. T. Madsen, O. Saba, B. Policeni, M. A. Howard, and W. R. K. Smoker, "A segmentation-based method for metal artifact reduction," *Academic Radiology*, vol. 14, no. 4, pp. 495–504, 2007.

[13] X. Duan, L. Zhang, Y. Xiao, J. Cheng, Z. Chen, and Y. Xing, "Metal artifact reduction in CT images by sinogram TV inpainting," in *Nuclear Science Symposium Conference Record*, 2008, pp. 4175–4177.

[14] G. van Kaick and S. Delorme, "Computed tomography in various fields outside medicine," *European Radiology Supplements*, vol. 15, pp. 74–81, 2005.

[15] "Toshiba Medical Systems Corporation Aquilion 32 `http://www.toshiba-medical.co.uk/ct-systems.asp` [Jan. 01, 2012]," .

[16] "GE Healthcare discovery CT750 HD `http://www.gehealthcare.com/euen/ct/products/` [Jan. 01, 2012]," .

[17] A. F. Kopp, K. Klingenbeck-Regn, M. Heuschmid, A. Kuttner, B. Ohnesorge, T. Flohr, S. Schaller, and C. D. Claussen, "Multislice computed tomography: basic principles and clinical applications," *Electromedica-Erlangen*, vol. 68, no. 2, pp. 94–105, 2000.

[18] N. E. L. Shanks and A. L. W. Bradley, *Handbook of Checked Baggage Screening: Advanced Airport Security Operation*, John Wiley and Sons, 2004.

[19] A. Buades, B. Coll, and J. M. Morel, "On image denoising methods," *SIAM Multiscale Modeling and Simulation*, vol. 4, no. 2, pp. 490–530, 2005.

[20] P. Perona and J. Malik, "Scale-space and edge detection using anisotropic diffusion," *IEEE Trans. on Pattern Analysis and Machine Intelligence*, vol. 12, no. 7, pp. 629–639, 1990.

[21] J. Canny, "A computational approach to edge detection," *IEEE Trans. on Pattern Analysis and Machine Intelligence*, , no. 6, pp. 679–698, 1986.

[22] L. I. Rudin, S. Osher, and E. Fatemi, "Nonlinear total variation based noise removal algorithms," *Physica D: Nonlinear Phenomena*, vol. 60, no. 1-4, pp. 259–268, 1992.

[23] A. Beck and M. Teboulle, "Fast gradient-based algorithms for constrained total variation image denoising and deblurring problems," *IEEE Trans. on Image Processing*, vol. 18, no. 11, pp. 2419–2434, 2009.

[24] G. Gilboa, N. Sochen, and Y. Y. Zeevi, "Texture preserving variational denoising using an adaptive fidelity term," in *Proc. Variational and Level Set Methods*, 2003, vol. 5, pp. 137–144.

[25] A. Chambolle, "An algorithm for total variation minimization and applications," *Journal of Mathematical Imaging and Vision*, vol. 20, no. 1, pp. 89–97, 2004.

[26] M. Zhang and B. K. Gunturk, "A new image denoising framework based on bilateral filter," in *Proc. SPIE*, 2008, vol. 6822, pp. 68221B–68221B–8.

[27] B. K. Gunturk, "Bilateral filter: Theory and applications," *Computational Photography: Methods and Applications*, vol. 2, pp. 339, 2010.

[28] C. Tomasi and R. Manduchi, "Bilateral filtering for gray and color images," in *Computer Vision, 1998. Sixth Inter. Conf. on*, 1998, pp. 839–846.

[29] S. Paris, P. Kornprobst, J. Tumblin, and F. Durand, "A gentle introduction to bilateral filtering and its applications," in *ACM SIGGRAPH 2007 courses*, 05-09 August 2007.

[30] R. R. Coifman, D. L. Donoho, A. Antoniadis, and G. Oppenheim, "Translation-invariant de-noising," *Wavelets and Statistics*, pp. 125–150, 1995.

[31] A. Buades, B. Coll, and J. M. Morel, "A non-local algorithm for image denoising," in *Proc. Conference on Computer Vision and Pattern Recognition*, 2005, vol. 2, pp. 60–65.

[32] B. Lichtenbelt, R. Crane, S. Naqvi, and Hewlett-Packard Company, *Introduction to volume rendering*, Prentice Hall PTR Upper Saddle River, NJ, 1998.

[33] Zhou Wang and A.C. Bovik, "Mean squared error: Love it or leave it? a new look at signal fidelity measures," *Signal Processing Magazine, IEEE*, vol. 26, no. 1, pp. 98 –117, jan. 2009.

[34] A. Mouton, N. Megherbi, G.T. Flitton, and T.P. Breckon, "A novel intensity limiting approach to metal artefact reduction in 3D CT baggage imagery," in *Proc. International Conference on Image Processing*. September 2012, IEEE, to appear.

[35] D. G. Lowe, "Object recognition from local scale-invariant features," in *Computer Vision. IEEE Inter. Conf. on*, 1999, vol. 2, pp. 1150–1157 vol. 2.